

Stabilization of one-dimensional Townes solitons by spin-orbit coupling in a dual-core system

Elad Shamriz^a, Zhaopin Chen^{a*} and Boris A. Malomed^{a,b}

^a*Department of Physical Electronics, School of Electrical Engineering,
Faculty of Engineering, and Center for Light-Matter Interaction,
Tel Aviv University, P.O.B. 39040, Ramat Aviv, Tel Aviv, Israel*

^b*Instituto de Alta Investigación, Universidad de Tarapacá, Casilla 7D, Arica, Chile*

It was recently demonstrated that 2D Townes solitons (TSs) in two-component systems with cubic self-focusing, which are normally made unstable by the critical collapse, can be stabilized by linear spin-orbit coupling (SOC), in Bose-Einstein condensates and optics alike. We demonstrate that 1D TSs, realized as optical spatial solitons in a planar dual-core waveguide with dominant quintic self-focusing, may be stabilized by SOC-like terms emulated by obliquity of the coupling between cores of the waveguide. Thus, SOC offers a universal mechanism for the stabilization of (quasi-) TSs. A combination of systematic numerical considerations and analytical approximations identifies a vast stability area for skew-symmetric solitons in the system's main (semi-infinite) and annex (finite) bandgaps. Tilted ("moving") solitons are unstable, spontaneously evolving into robust breathers. For broad solitons, diffraction, represented by second derivatives in the system, may be neglected, leading to a simplified model with a finite bandgap. It is populated by skew-antisymmetric gap solitons, which are nearly stable close to the gap's bottom.

1. Introduction

A well-known problem in studies of solitons (self-trapped modes in nonlinear dispersive/diffractive media) is that, if the focusing nonlinearity is too strong and/or underlying spatial dimension is too high, soliton solutions are destabilized by the presence of the collapse, i.e., catastrophic self-compression of wave fields in the same media [1, 2]. If the respective D -dimensional equation of the nonlinear-Schrödinger (NLS) type for complex field u contains a focusing term $\sim |u|^{2\sigma}u$ with real $\sigma > 0$, the critical collapse (the onset of which requires a norm of the field exceeding a certain threshold value) takes place at $\sigma D = 2$, and the supercritical collapse (which is possible with an arbitrarily small norm) occurs at $\sigma D > 2$ [1, 2]. Thus, the critical nonlinearity strength corresponds to $\sigma = 1$ (cubic) and $\sigma = 2$ (quintic) in the 2D and 1D geometries, respectively. A specific feature of the NLS equation with the critical nonlinearity is the existence of a degenerate family of *Townes solitons* (TSs), first found as 2D numerical solutions of the cubic NLS equation [3], and identified as a 1D analytical solution of the quintic equation [4, 5]. The families are degenerate in the sense that all the TSs share a common value of the integral norm, due to the fact that the NLS equation with the critical nonlinearity features a conformal invariance, allowing one to transform different TSs into each other, keeping the norm unaltered. The TSs are unstable solutions, which separate decaying and collapsing ones [1, 2]. In terms of the evolution of small perturbations, the TS instability is represented by zero eigenvalues, i.e., the instability is subexponential (but, nevertheless, quite tangible) [2].

Because the cubic focusing is a ubiquitous nonlinearity in optics (the Kerr effect) [6], plasmas (the nonlinearity of Langmuir waves [7]), atomic Bose-Einstein condensates, BECs (the cubic term in the Gross-Pitaevskii equation induced by attractive inter-atomic collisions [8]), etc., and all these settings naturally occur in the 2D form, a challenging problem is to modify the respective models by including additional physically relevant terms which may stabilize 2D solitons. In the course of theoretical and experimental work, various solutions of this problem were elaborated, as summarized in early reviews [9, 10] and updated ones [11–13]. In particular, these are higher-order defocusing nonlinearities (usually represented by quintic terms), which compete with the cubic focusing in optical media [14–16], and spatially-periodic potentials, induced by optical lattices in BEC or by photonic-crystal structures in optical waveguides. The periodic potentials readily stabilize both fundamental and vorticity-carrying 2D solitons [17, 18]. More recently, it was predicted [19–22], and experimentally demonstrated in various forms [24–28], that self-trapped 3D and quasi-2D states in binary BEC with attraction between its two components can be created in the form of stable "quantum droplets". They are filled by a nearly incompressible superfluid, being stabilized against the collapse by the effective quartic self-repulsion induced by the Lee-Huang-Yang (LHY) effect [23], i.e., a contribution of quantum Bogoliubov modes excited around the mean-field states. It was predicted too that 3D and 2D "droplets" with embedded vorticity may be stable as well [29, 30]. Furthermore, it was found theoretically and demonstrated experimentally

*Electronic address: viskoleczp@gmail.com

that the LHY effect helps to stabilize localized multidimensional states in BEC with long-range interactions between dipolar atoms [31–33, 33–35].

The current work on BEC has suggested another possibility to stabilize 2D and 3D solitons, namely, the use of the (pseudo-) spin-orbit-coupling (SOC), which was implemented, as a linear effect, in binary condensates [36–38]. It was demonstrated that, if linear SOC terms, which mix two BEC components via the first spatial derivatives (which represent the anomalous velocity in the condensate superfluid [39–41]), are added to the usual cubic intra- and inter-component attraction, they lift the above-mentioned conformal invariance, and thus allow the coupled NLS equations to create solitons with the norm falling below the fixed TS value. As a result, these solitons become stable (immune to the onset of the critical collapse). In particular, they restore the system's ground state, which is absent when the dynamics is dominated by the critical collapse [42, 43]. Furthermore, 2D solitons can be stabilized by the quasi-1D SOC, which is applied along a single direction in the 2D plane [44]. In the 3D setting, the supercritical collapse cannot be suppressed by the SOC terms; nevertheless, they help to make metastable solitons, which stay robust against small perturbations [45].

While the (pseudo-) SOC terms in BEC emulate genuine SOC, originally discovered in semiconductors, by mapping the spinor wave functions of electrons, moving in the ionic lattice, into a two-component mean-field bosonic wave function of the binary BEC, the latter setting may be, in turn, emulated by bimodal light propagation in optical waveguides. In particular, the above-mentioned mechanism stabilizing 2D matter-wave solitons can be reproduced for 2D spatiotemporal solitons in a dual-core planar waveguide (coupler) [46]. In the coupler model, two components of the binary BEC are replaced by optical fields in parallel tunnel-coupled cores with intrinsic Kerr (focusing cubic) nonlinearity in each core, while the SOC itself is emulated by temporal dispersion of the linear inter-core coupling. As a result, a family of stable 2D solitons was constructed. A similar but different optical model was proposed in Ref. [47], which was also based on the spatiotemporal propagation of light in a dual-core planar structure with the Kerr nonlinearity, but the SOC terms were emulated by spatial (rather than temporal) corrections to the linear inter-core coupling, produced by obliquity of the barrier separating the parallel cores.

The predicted stabilization of the two-component 2D solitons in the cubic self-focusing media by the optically emulated linear SOC terms suggests to consider a possibility to stabilize, by means of optically emulated SOC, 1D solitons of the quasi-TS type in a medium with quintic focusing, which, as mentioned above, is the critical nonlinearity in 1D (similarly to the cubic focusing in 2D, it also gives rise to the critical collapse). The objective of the present work is to introduce such a model (in the full form including paraxial diffraction, and its reduced diffractionless version), construct solitons in it, and investigate their stability. It is relevant to mention that peculiarities of the collapse of 1D solitons in the SOC model with quintic attraction were recently addressed in Ref. [41], but a possibility of stabilization was not considered there.

The model is introduced below in Section 2. As the preliminary stage of the analysis, spontaneous symmetry breaking (SSB) in the coupler with the quintic self-focusing in the absence of SOC is considered in Section 3. The main part of the work is reported in Section 4, *viz.*, systematic numerical results for families of skew-symmetric solitons stabilized by the (pseudo-) SOC. Gap solitons in the reduced model, which neglects the second spatial derivatives, are considered in Section 5. The paper is concluded by Section 6.

2. The model

We start by considering the propagation of optical waves in the planar dual-core guide described by coupled NLS equations for wave amplitudes (envelope functions) $u(z, x)$ and $v(z, x)$ in the two cores. In the scaled form, the NLS system is

$$iu_z + \frac{1}{2}u_{xx} + |u|^4u + \Lambda v = 0, \quad (1)$$

$$iv_z + \frac{1}{2}v_{xx} + |v|^4v + \Lambda u = 0, \quad (2)$$

where z and x are the propagation distance and transverse coordinate, Λ is the constant of the inter-core tunnel coupling, and it is assumed that the intrinsic self-focusing is represented by the quintic terms, which may be realized in colloidal optical waveguides. As shown by direct experiments [15, 16], the dominance of the quintic nonlinearity can be provided by selecting appropriate values of the size of metallic nanoparticles and their concentration in the colloid. The analysis clearly demonstrates that the results will not be essentially affected by a residual cubic nonlinearity, if any.

The remaining scaling invariance of Eqs. (1) and (2) makes it possible to fix $\Lambda \equiv 1$ (which implies that the propagation distance is measured in units of the coupling length), as set below.

The emulation of SOC is provided by corrections to the linear coupling in Eqs. (1) and (2) which are induced, as

in Ref. [47], by the skewness of the layer separating the guiding cores in the planar coupler:

$$iu_z + \frac{1}{2}u_{xx} + |u|^4u + v - \delta \cdot v_x = 0, \quad (3)$$

$$iv_z + \frac{1}{2}v_{xx} + |v|^4v + u + \delta \cdot u_x = 0, \quad (4)$$

where real $\delta > 0$ represents a shear between the cores in the skewed coupler, see Fig. 1 in [47]. It can be defined in terms of two components, $u(x)$ and $v(x)$, of the full modal eigenfunction of the dual-core waveguide: the respective overlap integral, $\int u_{\text{modal}}(x)v_{\text{modal}}^*(x - \Delta x)dx$ (with $*$ standing for the complex conjugate), attains a maximum when the inter-core shift takes value $\Delta x = \delta$. In comparison with the basic SOC models, the first x -derivatives in Eqs. (3) and (4) may be considered as emulating the anomalous velocity, while the second derivatives (the paraxial diffraction) correspond to the normal velocity [39, 40].

In the framework of the present model, stationary states with real propagation constant k are looked for by substituting

$$\{u, v\} = e^{ikz} \{U(x; \delta), V(x; \delta)\} \quad (5)$$

in equations (3) and (4) for the wave amplitudes. The corresponding equations for real functions $U(x; \delta)$ and $V(x; \delta)$ are

$$-kU + \frac{1}{2}\frac{d^2U}{dx^2} + U^5 + V - \delta \cdot \frac{dV}{dx} = 0, \quad (6)$$

$$-kV + \frac{1}{2}\frac{d^2V}{dx^2} + V^5 + U + \delta \cdot \frac{dU}{dx} = 0. \quad (7)$$

It is relevant to identify the spectrum of the linearized version of the present system. Looking for solutions to the linearization of Eqs. (6) and (7) in the form of plane waves,

$$\{U, V\} \sim \exp(iqx) \quad (8)$$

with wavenumber q , one derives the following dispersion relation between k and q^2 :

$$k = -(1/2)q^2 \pm \sqrt{1 + \delta^2 q^2}. \quad (9)$$

More convenient for the subsequent analysis is an inverted form of the relation:

$$q^2 = 2 \left(\delta^2 - k \pm \sqrt{\delta^4 - 2\delta^2 k + 1} \right). \quad (10)$$

The spectrum determined by Eqs. (9) and (10) includes *gaps*, i.e., intervals of propagation constant k in which the plane waves do not exist, hence they may be populated by solitons, in the framework of the full nonlinear system. In the case of $\delta^2 > 1$ (when the pseudo-SOC is strong enough), we identify the semi-infinite *main gap* as

$$k > k_{\text{max}} \equiv \frac{\delta^4 + 1}{2\delta^2}. \quad (11)$$

In this gap, expressions (10) are complex, hence the corresponding values of q are complex too, and solitons populating the gap will have oscillatory tails (see Fig. 7 below). In the case of $\delta^2 < 1$, there is an additional finite *annex gap*, adjacent to the main one,

$$1 < k < \frac{\delta^4 + 1}{2\delta^2}. \quad (12)$$

In the annex gap, both branches of expression (10) are real negative ones, which makes the respective values of q purely imaginary, hence the respective solitons should have tails monotonously decaying at $|x| \rightarrow \infty$, see Fig. 8 below. A given value of the propagation constant, $k > 1$, belongs to the annex gap (12) for values of the pseudo-SOC strength

$$\delta^2 < k - \sqrt{k^2 - 1}. \quad (13)$$

Generic examples of the dispersion curves with $\delta^2 < 1$ and $\delta^2 > 1$ are displayed in Fig. 1. In the latter case, the largest value k_{max} of k , defined by Eq. (11), is attained at $q = \pm \sqrt{\delta^2 - 1/\delta^2}$.

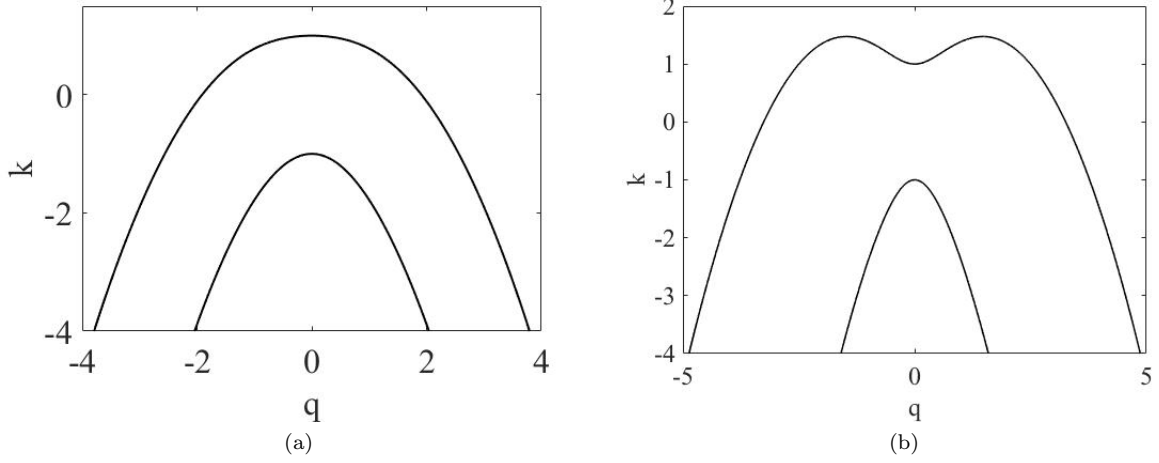


FIG. 1: The dispersion curves produced by Eq. (9) with $\delta = 0.8$ (a) and $\delta = 1.6$ (b).

In the absence of SOC, a coupled system with the opposite (defocusing) sign of the quintic nonlinearity, competing with cubic focusing, was considered in work [48], which addressed phenomenology of spontaneous symmetry breaking (SSB) of two-component solitons in the symmetric system. In that system, symmetric solitons in the absence of SSB, as well as asymmetric ones generated by SSB, may be stable due to the absence of the critical collapse.

The SOC-emulating terms in Eqs. (3) and (4) break the Galilean invariance of the system, therefore generation of “moving” solutions (in fact, spatial beams tilted in the (x, z) plane) from their “quiescent” counterparts (straight beams in the same plane) is a nontrivial issue. For this purpose, it is relevant to rewrite Eqs. (3) and (4) in terms of z and the tilted coordinate,

$$\xi \equiv x - cz, \quad (14)$$

where “velocity” c determines the obliquity of the beams in the spatial domain:

$$\begin{aligned} iu_z - icu_\xi + \frac{1}{2}u_{\xi\xi} + |u|^4u + v - \delta \cdot v_\xi &= 0, \\ iv_z - icv_\xi + \frac{1}{2}v_{\xi\xi} + |v|^4v + u + \delta \cdot u_\xi &= 0. \end{aligned} \quad (15)$$

Further, the “tilted” system (15) may be simplified by the following transformation, which is suggested by the Galilean boost in systems which are Galilean invariant:

$$\{u(\xi, z), v(\xi, z)\} \equiv \exp\left(\frac{i}{2}c^2z + ic\xi\right) \{\tilde{u}(\xi, z), \tilde{v}(\xi, z)\}. \quad (16)$$

This transformation casts the equations in the following form:

$$\begin{aligned} i\tilde{u}_z + \frac{1}{2}\tilde{u}_{\xi\xi} + |\tilde{u}|^4\tilde{u} + (\Lambda - ic\delta)\tilde{v} - \delta \cdot \tilde{v}_\xi &= 0, \\ i\tilde{v}_z + \frac{1}{2}\tilde{v}_{\xi\xi} + |\tilde{v}|^4\tilde{v} + (\Lambda + ic\delta)\tilde{u} + \delta \cdot \tilde{u}_\xi &= 0. \end{aligned} \quad (17)$$

Stationary solutions to Eq. (17) may be sought for as $\{\tilde{u}, \tilde{v}\} = e^{ikz} \{\tilde{U}(\xi), \tilde{V}(\xi)\}$, cf. Eq. (5), with complex functions $\tilde{U}(\xi)$ and $\tilde{V}(\xi)$ satisfying equations

$$-k\tilde{U} + \frac{1}{2}\frac{d^2\tilde{U}}{d\xi^2} + |\tilde{U}|^4\tilde{U} + (1 - ic\delta)\tilde{V} - \delta\frac{d\tilde{V}}{d\xi} = 0, \quad (18)$$

$$-k\tilde{V} + \frac{1}{2}\frac{d^2\tilde{V}}{d\xi^2} + |\tilde{V}|^4\tilde{V} + (1 + ic\delta)\tilde{U} + \delta\frac{d\tilde{U}}{d\xi} = 0. \quad (19)$$

The underlying system of coupled NLS equations (1) and (2) conserves the total norm, Hamiltonian, and momentum:

$$N \equiv N_u + N_v = \int_{-\infty}^{+\infty} \left[|u(x)|^2 + |v(x)|^2 \right] dx, \quad (20)$$

$$H = \int_{-\infty}^{+\infty} \left[\frac{1}{2} (|u_x|^2 + |v_x|^2) - \frac{1}{3} (|u|^6 + |v|^6) - (uv^* + u^*v) + \frac{\delta}{2} (u^*v_x + uv_x^* - u_x^*v - u_xv^*) \right] dx, \quad (21)$$

$$P = i \int_{-\infty}^{+\infty} (u_x^*u + v_x^*v) dx. \quad (22)$$

Note that momentum (22) is conserved in spite of the lack of the Galilean invariance of the system.

3. Asymmetric solitons in the absence of the spin-orbit coupling (SOC), $\delta = 0$

3.1. The spontaneous-symmetry-breaking (SSB) point of two-component solitons

Before presenting results for solitons under the action of the pseudo-SOC, it is relevant to briefly address ones in the system of Eqs. (1) and (2) in the absence of SOC. As mentioned above, in that case the issue of basic interest is the SSB of two-component solitons in the symmetric system [49]-[54].

For symmetric solitons, with $U(x) = V(x) \equiv U_0(x)$, Eqs. (6) and (7) with $\delta = 0$ reduce to a single equation:

$$-(k-1)U_0 + \frac{1}{2} \frac{d^2 U_0}{dx^2} + U_0^5 = 0. \quad (23)$$

The exact solution to Eq. (23), which represents the 1D (*quasi*) version of the TS (Townes' soliton), exists for $k > 1$:

$$U_0(x) = \frac{[3(k-1)]^{1/4}}{\sqrt{\cosh(2\sqrt{2(k-1)}x)}}. \quad (24)$$

In agreement with the above-mentioned fundamental property of TSs, the norm of solution (20) takes a single value which does not depend on k :

$$N_{\text{TS}} = \sqrt{3/2}\pi. \quad (25)$$

Only the symmetric solitons exist at $k < k_{\text{cr}}$, while asymmetric ones appear at $k > k_{\text{cr}}$. The critical value k_{cr} can be found exactly, by looking for a solution with a vanishingly small asymmetric part, as

$$(U(x), V(x)) = U_0(x) \pm \epsilon \delta U(x), \quad (26)$$

where ϵ is an infinitely small amplitude, which accounts for the onset of the SSB. Straightforward analysis, which follows that developed earlier for the coupler with the cubic nonlinearity [49, 52], demonstrates that $\delta U(x)$ satisfies the following linear equation:

$$\left[\frac{1}{2} \frac{d^2}{dx^2} + \frac{15(k-1)}{\cosh^2(2\sqrt{2(k-1)}x)} \right] \delta U = (k+1) \delta U. \quad (27)$$

Making use of the known exact solutions for the linear Schrödinger equation with the Pöschl-Teller potential [55], we find the SSB point from a solution of Eq. (27):

$$k_{\text{cr}} = 5/4. \quad (28)$$

In addition to the symmetric and asymmetric soliton solutions, Eqs. (6) and (7) admit antisymmetric ones, with $U(x; \delta) = -V(x; \delta)$. However, they are subject to strong instability, which is driven by the fact that the coupling term in Hamiltonian (21) is positive for the antisymmetric solutions, on the contrary to the negative one for the symmetric solitons [54]. Further, the analysis similar to that leading to Eq. (27) demonstrates that the antisymmetric solitons do not undergo a bifurcation of antisymmetry breaking (the same happens in the coupler with the cubic nonlinearity [54]).

3.2. The variational approximation (VA) for the asymmetric solitons

At $k > k_{\text{cr}}$, asymmetric solitons cannot be found in an exact form, but it is possible to approximate them by means of the variational method, cf. works [50]-[53] for the coupler with the cubic nonlinearity (see also a review in [54]). To this end, we note that Eqs. (6) and (7) with $\delta = 0$ can be derived from the following Lagrangian:

$$L = \int_{-\infty}^{+\infty} \left\{ \frac{k}{2} (U^2 + V^2) + \frac{1}{4} \left[\left(\frac{dU}{dx} \right)^2 + \left(\frac{dV}{dx} \right)^2 \right] - \frac{1}{6} (U^6 + V^6) - UV \right\} dx, \quad (29)$$

cf. Hamiltonian (21) with $\delta = 0$. The VA can be applied, using an ansatz whose form is suggested by solution (24):

$$(U, V) = \frac{A(\cos \theta, \sin \theta)}{\sqrt{\cosh(ax)}}, \quad (30)$$

where A and a determine the amplitude and inverse width of the soliton, while its asymmetry is determined by a parameter which measures the relative difference of the norms of the two components, see Eq. (20):

$$\Theta \equiv \frac{N_u - N_v}{N_u + N_v} = \cos(2\theta) \quad (31)$$

The total norm of this ansatz, $N = \pi A^2/a$, does not depend on θ . Below, the amplitude is eliminated in favor of N , using this relation.

The substitution of ansatz (30) in the Lagrangian and subsequent integration produces the following result:

$$L(N, a, \theta) = \frac{k}{2} N + \frac{Na^2}{32} - \frac{N^3 a^2}{96\pi^2} [5 + 3 \cos(4\theta)] - \frac{N}{2} \sin(2\theta), \quad (32)$$

The variational (Euler-Lagrange) equations, $\partial L / \partial(2\theta) = \partial L / \partial a = \partial L / \partial N = 0$ yield, after some algebra, the following results for asymmetric solitons, with $\cos(2\theta) \neq 0$:

$$\Theta(N) = \sqrt{(1/3) \left[(N_{\text{TS}}/N)^2 - 1 \right]}, \quad (33)$$

$$a^2(N) = \frac{2\pi^2 \sqrt{3}}{N^2 \sqrt{1 - (N_{\text{TS}}/2N)^2}}, \quad (34)$$

$$k(N) = \frac{2}{\sqrt{3 \left[1 - (N_{\text{TS}}/2N)^2 \right]}}. \quad (35)$$

where N_{TS} is the 1D-TS norm (25). Thus, it is expected that the asymmetric solitons exist with norms taking values which secure the positiveness of the expression under the square root in Eqs. (34) and (35), and fulfillment of condition $0 \leq \cos^2(2\theta) \leq 1$, in interval

$$N_{\text{TS}}/2 < N < N_{\text{TS}}. \quad (36)$$

It is easy to see that this existence interval is an exact one (without the reference to the VA), with $\Theta(N = N_{\text{TS}}/2) = 1$, $k(N = N_{\text{TS}}/2) = \infty$, and $\Theta(N = N_{\text{TS}}) = 0$, $k(N = N_{\text{TS}}) = 5/4$ (see Eq. (28)).

Note that the TS norm for the single 1D NLS equation with the quintic self-focusing term (i.e., Eq. (1) with $\Lambda = 0$) is half of the value given by Eq. (25), hence development of instability of asymmetric solitons with the norm belonging to interval (36) may result in either decay of the soliton or the onset of the collapse in one core, see Figs. 5 and 6 below. In this connection, it is relevant to mention that the VA predicts that the norm in one core (normalized to $N_{\text{TS}}/2$), which is

$$\frac{N_u}{N_{\text{TS}}/2} \equiv \frac{N}{N_{\text{TS}}/2} \cos^2 \theta = \frac{N}{N_{\text{TS}}} + \sqrt{\frac{1}{3} \left(1 - \frac{N^2}{N_{\text{TS}}^2} \right)}, \quad (37)$$

pursuant to the definition of ansatz (30) and Eq. (33), attains a maximum, $(2N/N_{\text{TS}})_{\text{max}} = 2/\sqrt{3}$, at $N = (\sqrt{3}/2) N_{\text{TS}}$, the respective value of the propagation constant being

$$k(N/N_{\text{TS}} = 1/\sqrt{3}) = \sqrt{2}. \quad (38)$$

Thus, the VA predicts that the asymmetric solitons emerge *subcritically*, at $N = N_{\text{TS}}/2$, with the largest degree of the asymmetry, $\Theta(N = N_{\text{TS}}/2) = 1$, attained at the diverging propagation constant, $k \rightarrow \infty$, as per Eq. (35). As shown in Fig. 2(a), with the increase of N from $N_{\text{TS}}/2$ to N_{TS} , the asymmetry decreases, following Eq. (33), and vanishes when the norm attains the TS value, $\Theta(N = N_{\text{TS}}) = 0$, the respective propagation constant, as predicted by the variational equation (35), being $k_{\text{cr}} = k(N = N_{\text{TS}}) = 4/3$ (to be compared to the exact value $5/4$, see Eq. (28), i.e., the relative inaccuracy of the VA is $\approx 6\%$). This picture, which may be identified as a *fully subcritical* SSB bifurcation (similar to the “fully backward” one found as an exact solution of the 1D NLS equation with the cubic self-focusing term multiplied by a symmetric pair of delta-functions, $\delta(x-a) + \delta(x+a)$ [56]), is drastically different from the *weakly subcritical* SSB bifurcation of solitons in the coupler with the cubic self-focusing, that gives rise to a pair of background-going branches of asymmetric unstable states, which quickly turn forward as stable branches [53, 54]. The branches of asymmetric solitons merge with the one of symmetric states at $N = N_{\text{TS}}$, and, naturally, no solitons exist at $N > N_{\text{TS}}$, as the presence of the collapse does not allow the existence of solitons with a supercritical norm. An essential difference from the bifurcation diagram reported in Ref. [56] is that, in the present system, all symmetric solitons (TSs), having the single value of the norm, $N = N_{\text{TS}}$, are represented by the single point in Fig. 2(a).

The monotonously decreasing dependence $k(N)$, predicted by the VA in the form of Eq. (35) (Fig. 2(b)), contradicts the well-known Vakhitov-Kolokolov criterion, $dk/dN > 0$, which is a necessary stability condition for solitons [1, 2, 57], hence the entire family of the asymmetric solitons is unstable (similar to what was found for the case of the fully backward bifurcation in [56]).

3.3. Numerical results for the asymmetric solitons

The predictions of the VA for the family of asymmetric solitons, *viz.*, dependences of the asymmetry parameter and propagation constant on the total norm, are compared to their counterparts, found from the numerical solution of Eq. (23), in Fig. 2. The comparison corroborates the accuracy of the approximation.

Typical examples of strongly and moderately asymmetric solitons, as produced by the VA and numerical solution, are displayed in Figs. 3 and 4, and their dynamical instability is shown in Figs. 5 and 6, respectively. The instability was identified in direct simulations, as well as via numerical calculation of eigenvalues λ of modes of small perturbations, produced by the linearization of Eqs. (1) and (2) (i.e., Bogoliubov - de Gennes equations, in terms of the SOC emulation). The perturbation modes were taken, as usual, as a combination of terms $\sim \exp(-i\lambda z)$ and $\exp(i\lambda^* z)$ [58]. The “normal” exponentially growing instability is determined by $|\text{Im}(\lambda)|$ in the case when complex eigenvalues are found. On the other hand, as mentioned above, the subexponential (but, nevertheless, tangible) instability of TSs is accounted for by zero eigenvalues [2].

In Fig. 5 it is observed that the instability of the strongly asymmetric soliton with a relatively small norm leads to decay, while the less asymmetric one with a higher norm suffers the collapse in Fig. 6. This difference is explained by the fact that, in the former case (with $k = 3$), Eq. (37) yields the norm in the dominant core which only slightly exceeds the single-core critical value: $N_u/(N_{\text{TS}}/2) \approx 1.027$. On the other, in the latter case (with $k = 1.8$, which is closer to the “most unstable” value (38)), the same ratio is ≈ 1.090 , making it possible to initiate the collapse, as observed in Fig. 6.

In the next section, we demonstrate that the inclusion of the SOC terms in Eqs. (1) and (2) may stabilize the symmetric TSs which are subject to the above-mentioned subexponential instability, and thus create the missing ground state in the system. On the other hand, it is not expected that the SOC is able to suppress the strong instability of the asymmetric solitons, which is accounted for by nonzero imaginary parts of eigenvalues λ , see Figs. 5(c) and 6(c). Therefore, in the subsequent analysis we focus on the stabilization of solitons which are symmetric TSs in the absence of SOC.

4. Stabilization of skew-symmetric solitons by the emulated SOC

4.1. The definition of the skew symmetry

It is easy to see that stationary equations (6) and (7) including the SOC-emulating terms with $\delta > 0$ are compatible with the *skew-symmetry* constraint,

$$U(x; \delta) = V(-x; \delta), \quad (39)$$

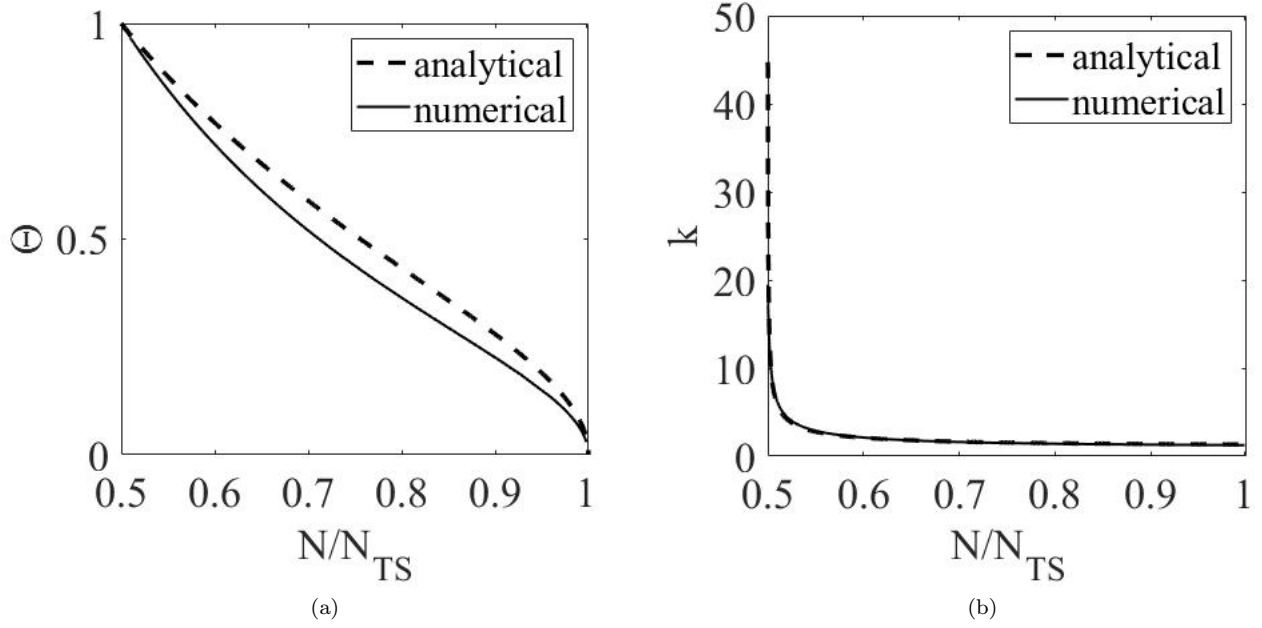


FIG. 2: Asymmetric solitons in the absence of SOC ($\delta = 0$). (a) Asymmetry parameter Θ , defined as per Eq. (31): the analytical prediction of the VA (variational approximation), given by Eq. (33), and its counterpart, produced by numerical solution of Eqs. (6) and (7), vs. the scaled norm. In this diagram, all symmetric (*quasi-Townes*) solitons are represented by the single point, $(N/N_{TS} = 1, \Theta = 0)$. (b) The propagation constant of the asymmetric soliton vs. its total norm: the analytical VA prediction, given by Eq. (35), and its numerical counterpart, vs. the scaled norm. Exact symmetric solitons (24) are actually represented in panel (b) by the right edge of the frame, corresponding to $N/N_{TS} = 1$, at $k > 1$, which intersects the branch of the asymmetric solutions at $k = 5/4$, according to Eq. (28).

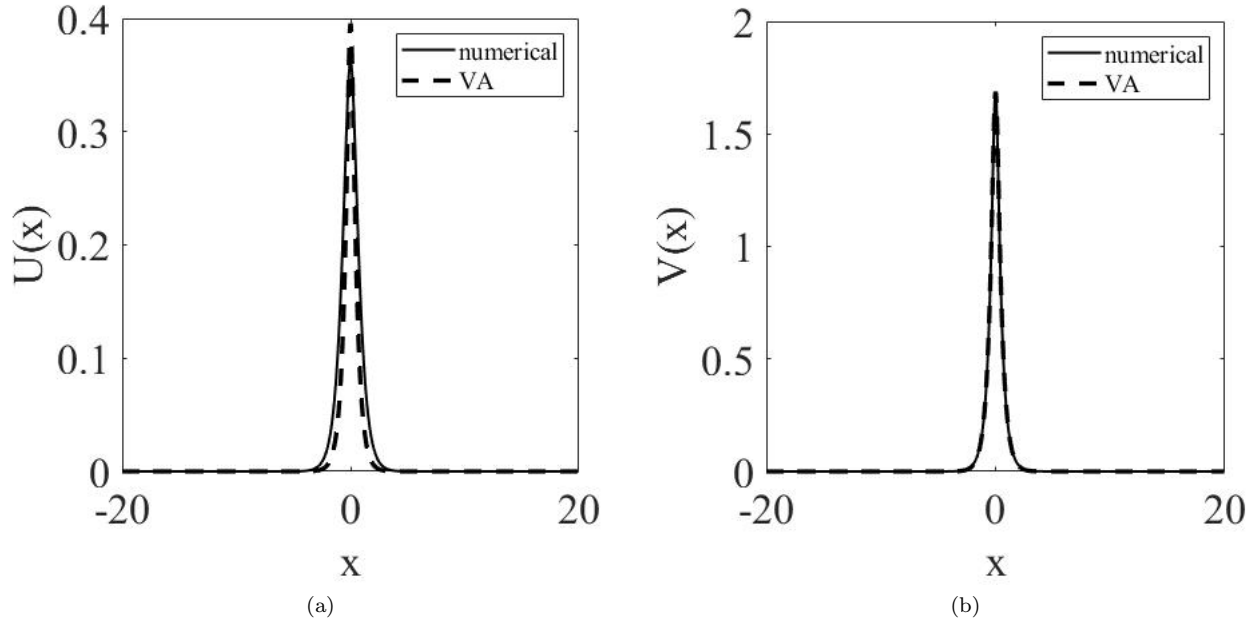


FIG. 3: An example of a strongly asymmetric soliton in the system without SOC ($\delta = 0$), as predicted by the VA based on Eqs. (30) and (33)-(35), and found in the numerical form. Note the difference in vertical scales between (a) and (b). The propagation constant is $k = 3$, the respective VA-predicted scaled norm being $(N/N_{TS})_{VA} \approx 0.541$, while its numerically found counterpart is $(N/N_{TS})_{num} \approx 0.545$.

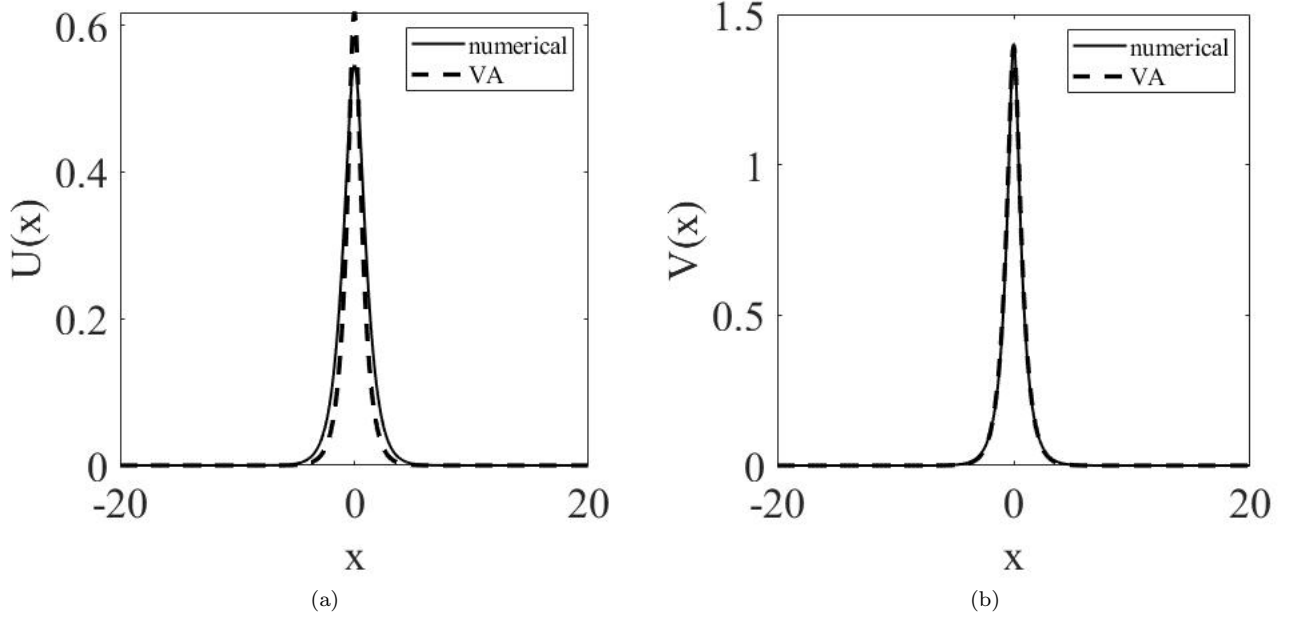


FIG. 4: The same as in Fig. 3, but for a less asymmetric soliton, corresponding to $k = 1.8$. In this case, $(N/N_{\text{TS}})_{\text{VA}} \approx 0.651$, and its numerically found counterpart is $(N/N_{\text{TS}})_{\text{num}} \approx 0.648$.

which replaces the symmetry condition occurring in the absence of SOC. This constraint is somewhat similar to skew and cross symmetries considered in models based on lattice potentials [59, 60]. In other words, constraint (39) means that $U(x, \delta) + V(x, \delta)$ and $U(x, \delta) - V(x, \delta)$ are, respectively, even and odd functions of x .

Unlike the symmetric solitons available in the analytical form (24), no exact solutions can be found in the presence of $\delta > 0$. However, treating the SOC strength δ as a small parameter, it is possible to look for solutions of Eqs. (6) and (7) perturbatively,

$$\{U(x), V(x)\} = \{U_0(x), V_0(x)\} + \delta \{U_1(x), V_1(x)\}, \quad (40)$$

where $\{U_0(x), V_0(x)\}$ is the solution (not necessarily the symmetric one) for $\delta = 0$. The substitution of ansatz (40) in Eqs. (6) and (7) and linearization with respect to small perturbations leads to the inhomogeneous equations:

$$\begin{aligned} \left(\frac{1}{2} \frac{d^2}{dx^2} - k + 5U_0(x) \right) U_1 + V_1 &= \frac{dV_0}{dx}, \\ \left(\frac{1}{2} \frac{d^2}{dx^2} - k + 5V_0(x) \right) V_1 + U_1 &= -\frac{dU_0}{dx}. \end{aligned} \quad (41)$$

Applying d/dx to Eqs. (6) and (7), and comparing the results to Eqs. (41), it is easy to find an *exact solution* of the latter equations, which contains an arbitrary parameter representing an infinitesimal shift of the soliton's center of mass. Keeping the shift equal to zero, one obtains the following exact solution to Eqs. (41):

$$\begin{aligned} U_1(x) &= -\frac{N_v \delta}{N_u + N_v} \frac{dU_0}{dx}, \\ V_1(x) &= \frac{N_u \delta}{N_u + N_v} \frac{dV_0}{dx}, \end{aligned} \quad (42)$$

where $N_{u,v}$ are norms of the two components at $\delta = 0$, see Eq. (20). Actually, as said above, the relevant case (when the solitons may be stabilized by SOC) is the one with the symmetric soliton at $\delta = 0$. In this case, solution (42) simplifies to

$$U_1(x) = -V_1(x) = -\frac{\delta}{2} \frac{dU_0}{dx}, \quad (43)$$

with $U_0(x)$ taken as per Eq. (24). This analytical approximation is compared to the numerical results (for $\delta = 0.35$, which is not a very small value) below in Fig. 8(c,d).

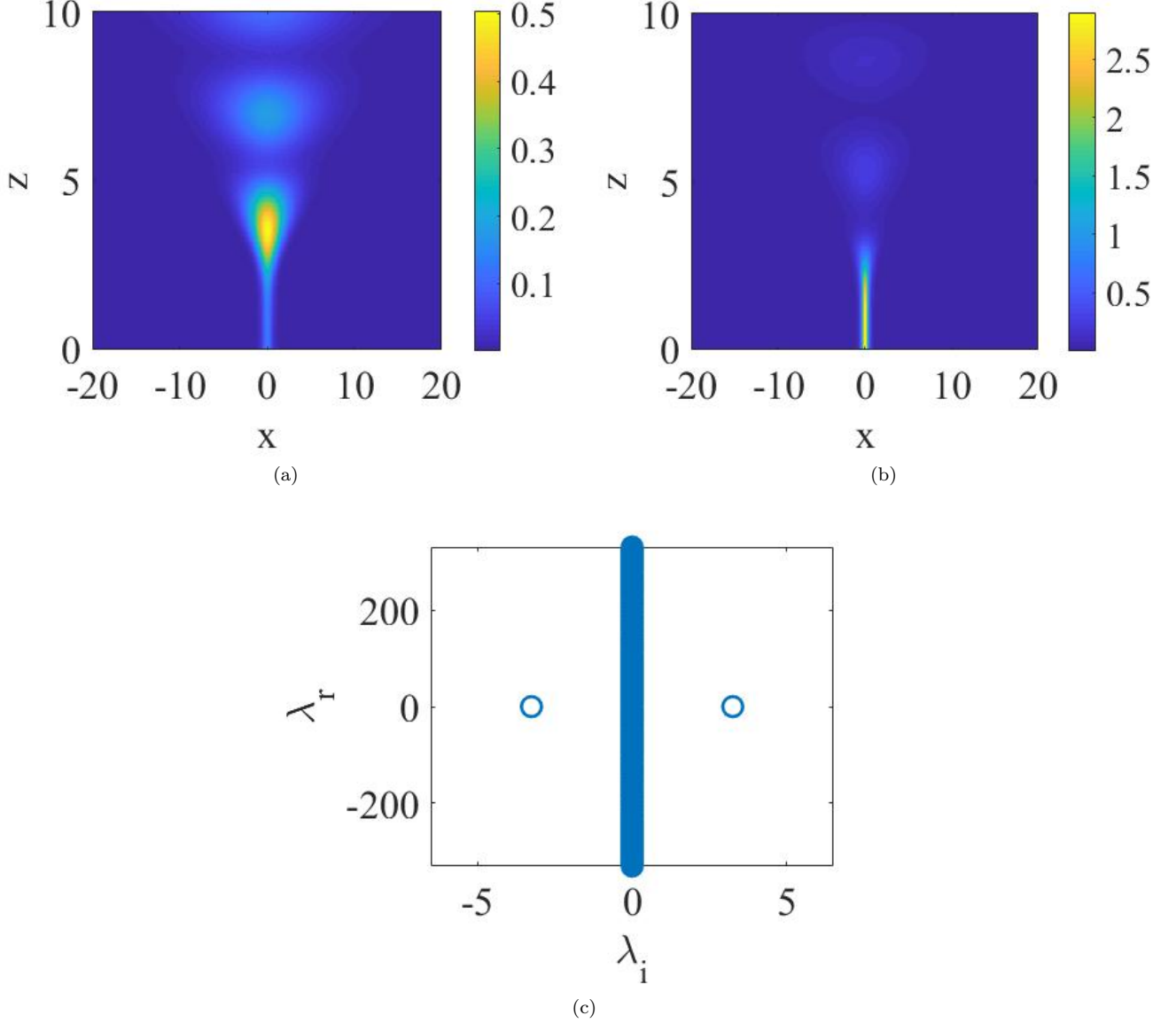


FIG. 5: The instability of the asymmetric soliton from Fig. 3. Panels (a) and (b) display, by means of contour plots, the decay of components $|u(x, z)|^2$ and $|v(x, z)|^2$, respectively. (c) The spectrum of eigenvalues of small perturbations added to the stationary soliton, as produced by the numerical solution of the linearized equations for small perturbations.

4.2. Skew-symmetric solitons and their stability

Localized solutions of coupled equations (6) and (7) obeying condition (39) were obtained in a numerical form. Generic examples of stable solitons belonging to the main and annex bandgaps, defined as per Eqs. (11) and (12), are presented in Figs. 7 and 8, respectively. The former solution features zero crossings, in accordance with the fact that, as mentioned above, wavenumber q of its tail, given by Eqs. (8) and (10), is complex, $q = q_r + iq_i$, hence the solution decays non-monotonously at $|x| \rightarrow \infty$: $\{U, V\} \sim \exp(-|q_i||x|) \cos(q_r x)$. The first zero-crossing is predicted by this estimate at

$$|x_0| = \pi / (2|q_r|). \quad (44)$$

In the case shown in Fig. 7, with $k = 1.2$, Eq. (10) yields $q_r \approx 0.81$ and $q_i \approx 0.93$. The first zero-crossing is observed in Fig. 7 at $|x_0| \approx 2.34$, while Eq. (44) gives $|x_0| \approx 2.3$, in agreement with the numerical findings. On the other hand, Eq. (10) yields purely imaginary q in the annex bandgap (12), hence the respective soliton's shape features

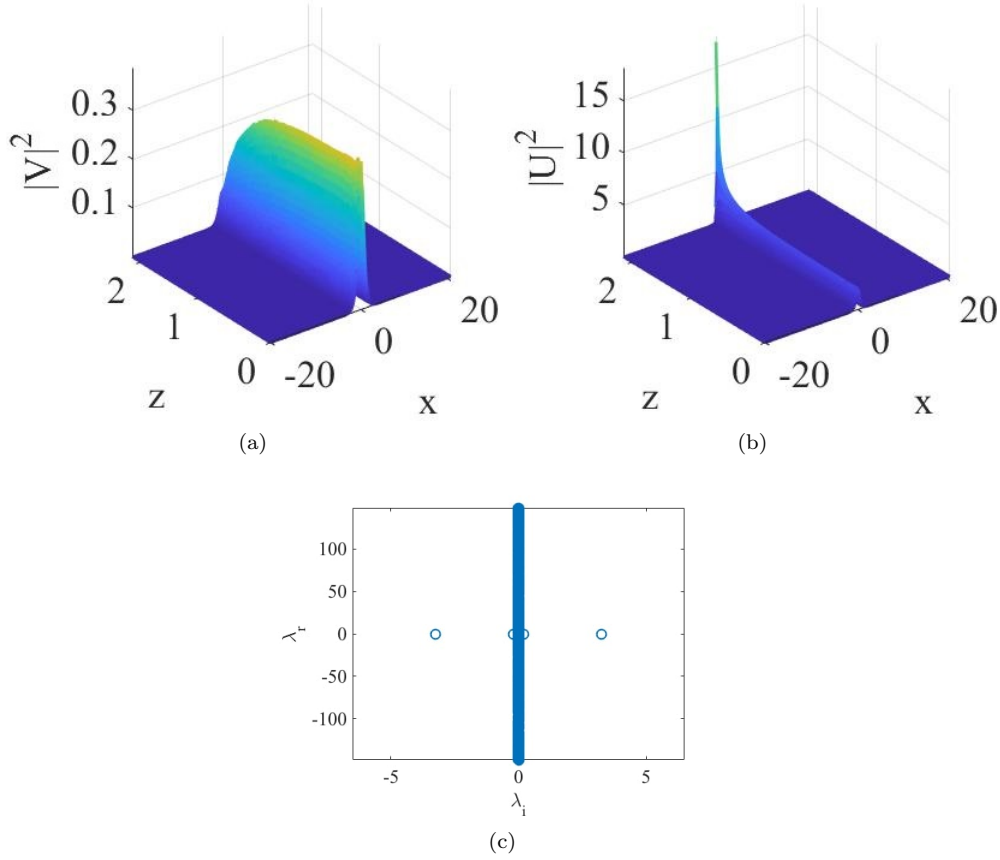


FIG. 6: The collapse instability of the soliton from Fig. 4. The meaning of the panels is the same as in Fig. 5, with the difference that the evolution of the two components is displayed, in panels (a) and (b), by means of the three-dimensional plots (note the difference in vertical scales in (a) and (b)).

monotonous decay of the tails at $|x| \rightarrow \infty$ and, accordingly, no zero crossings are observed in Fig. 8.

Results for the existence and stability of the skew-symmetric solitons are summarized in Fig. 9. The stability was identified by means of numerical calculation of eigenvalues for modes of small perturbations, and verified by direct simulations. In particular, the bottom existence boundary in panel 9(a) is determined by Eqs. (12) and (11). Further, the coordinate $k \approx 1.265$ of corner point C on the boundary between the stability and instability areas in the same panel may be explained by the above analytical result, according to which the symmetry-breaking instability of the solitons in the absence of SOC sets it at point (28), i.e., $k = 1.25$.

The key point, which explains the stabilization of the quasi-TS by SOC as a result of pushing the soliton's norm below its critical value for the TSs in the absence of SOC (see Eq. (25)), is illustrated by Figs. 9(c,d), which show that, for a fixed propagation constant, the norm of the skew-symmetric solitons indeed decreases with the increase of the SOC strength, δ , leading to the stabilization of the solitons. In this connection, it is relevant to mention that, as long as k belongs to the annex gap (12), in the limit of $k \rightarrow 1$ the stationary equations may be asymptotically reduced to Eqs. (6), (7) with $\delta = 0$ and the effective diffractive coefficient, taken from the expansion of the top branch of the dispersion relation (9) at $k \rightarrow 1$:

$$D \equiv -\frac{d^2 k}{dq^2} \Big|_{q=0} = 1 - \delta^2.$$

Then, the total norm of the soliton can be obtained from the TS value (25) by dint of straightforward renormalization:

$$N_{\text{asympt}}(k \rightarrow 1; \delta) = \sqrt{1 - \delta^2} N_{\text{TS}} = \sqrt{1 - \delta^2} \sqrt{3/2\pi}. \quad (45)$$

In particular, for $\delta = 0.8$, Eq. (45) yields $N(k \rightarrow 1; \delta = 0.8) \approx 2.31$, which is very close to the corresponding numerical value in Fig. 9(d), $N_{\text{numer}}(k \rightarrow 1; \delta = 0.8) \approx 2.32$.

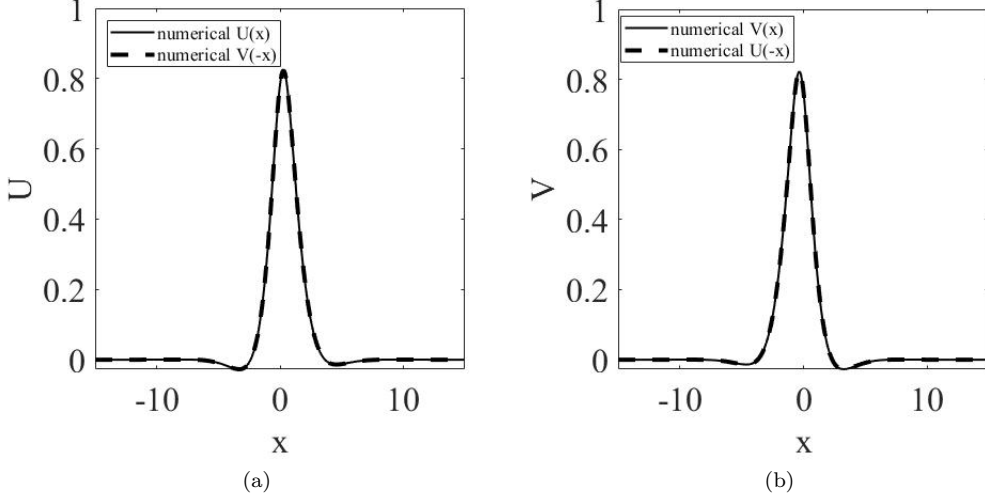


FIG. 7: The profile of a stable skew-symmetric soliton, corresponding to points A ($\delta = 1$) in Figs. 9(a,b). The soliton belongs to the main spectral gap. Its propagation constant and total norm are $k = 1.2$ and $N = 2.29$. The juxtaposition of profiles $U(\pm x)$ and $V(\mp x)$ in panels (a) and (b) corroborates that the soliton obeys the skew-symmetry constraint (39).

Equations (6) and (7) are also compatible with the constraint of the *skew antisymmetry*,

$$U(x; \delta) = -V(-x; \delta), \quad (46)$$

cf. Eq. (39) (in other words, the corresponding combinations $U(x) + V(x)$ and $U(x) - V(x)$ are, respectively, odd and even functions of x). Because solutions obeying Eq. (46) extend the above-mentioned strongly unstable antisymmetric solitons existing at $\delta = 0$, it is expected that the skew-antisymmetric solitons inherit the strong instability, therefore they are not considered in this section. Nevertheless, they are addressed in the next section dealing with the simplified diffractionless system, where skew-symmetric solutions do not exist.

4.3. Tilted skew-symmetric solitons

“Moving” (tilted) solitons have been found as numerical solutions of Eqs. (18) and (19), see Figs. 10(a,b). Unlike the “quiescent” (straight) solitons, the calculation of eigenvalues in the framework of the respective linearized equations demonstrates that all tilted solitons are unstable, see Fig. 10(c). Nevertheless, for sufficiently small values of the “velocity” (tilt) c , the instability is weak, the respective eigenvalues being complex in Fig. 10(c), rather than purely imaginary, cf. Figs. 5(c) and 6(c). As shown in Figs. 10(d,e), in direct simulations the weak instability does not destroy the solitons, but rather transforms them into breathers which feature robust intrinsic vibrations, with period $Z_{\text{breather}}^{(\text{numer})} \approx 40$ in this example. Note that the real part of the complex eigenvalues in Fig. 10(e), $\lambda_r \simeq \pm 0.136$, correctly predicts the period of the intrinsic vibrations in panels 10(a,b), as $Z_{\text{breather}}^{(\text{analyt})} = 2\pi/|\lambda_r| \approx 46$. It is also relevant to compare the vibration period with a characteristic diffraction length, $Z_{\text{diffr}} \simeq 8$, determined by the input soliton profile, the result being $Z_{\text{breather}} \simeq 5Z_{\text{diffr}}$ (i.e., the vibrations may be considered as a long-period dynamical feature). Figures 10(a,b) additionally demonstrate secondary small-amplitude short-period oscillations on top of the primary vibrations. This effect may be construed as the fifth harmonic of the fundamental frequency λ_r , generated by the quintic nonlinearity of the system.

At larger values of tilt c , solitons are subject to stronger instability, which quickly destroys them in direct simulations (not shown here in detail).

5. Gap solitons in the diffractionless limit

5.1. The simplified system

In the case when the effective diffraction induced by the SOC terms in Eqs. (3) and (4) is much stronger than the direct paraxial diffraction (in terms of the SOC emulation, this condition means that the anomalous velocity dominates over the normal one), the underlying system may be reduced to a simpler form, in which the second derivatives are

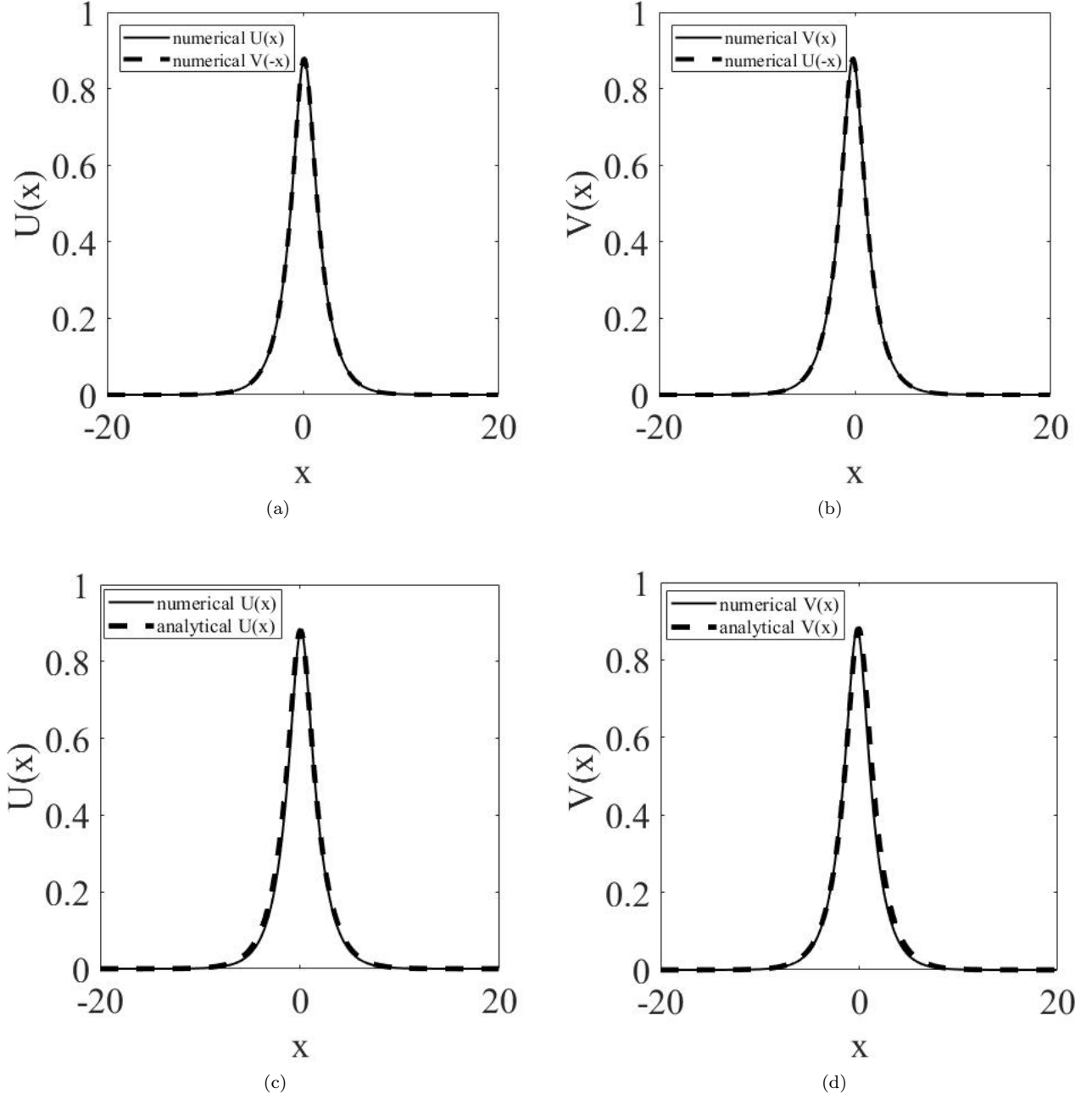


FIG. 8: The profile of a stable skew-symmetric soliton corresponding to points B ($\delta = 0.35$) in Figs. 9(a,b). The soliton belongs to the annex gap. Its propagation constant and total norm are $k = 1.2$ and $N = 3.61$. (a,b) The juxtaposition of profiles $U(\pm x)$ and $V(\mp x)$ in panels (a) and (b) corroborates that the soliton obeys the skew-symmetry constraint (39). (c,d) Comparison between the analytical approximation given by Eqs. (40), (43) and the numerical solution of Eqs. (7) and (6). To estimate the relative size of the analytical correction given by Eq. (43), we note that, at the point where the local intensity of solution (24), $U_0^2(x)$, is half of its maximum value, Eq. (43) with $\delta = 0.35$ and $k = 1.2$ yields $|U_1/U_0| \approx 0.1$.

dropped, cf. Refs. [61] and [62]:

$$iu_z - v_x + |u|^4 u + v = 0, \quad (47)$$

$$iv_z + u_x + |v|^4 v + u = 0. \quad (48)$$

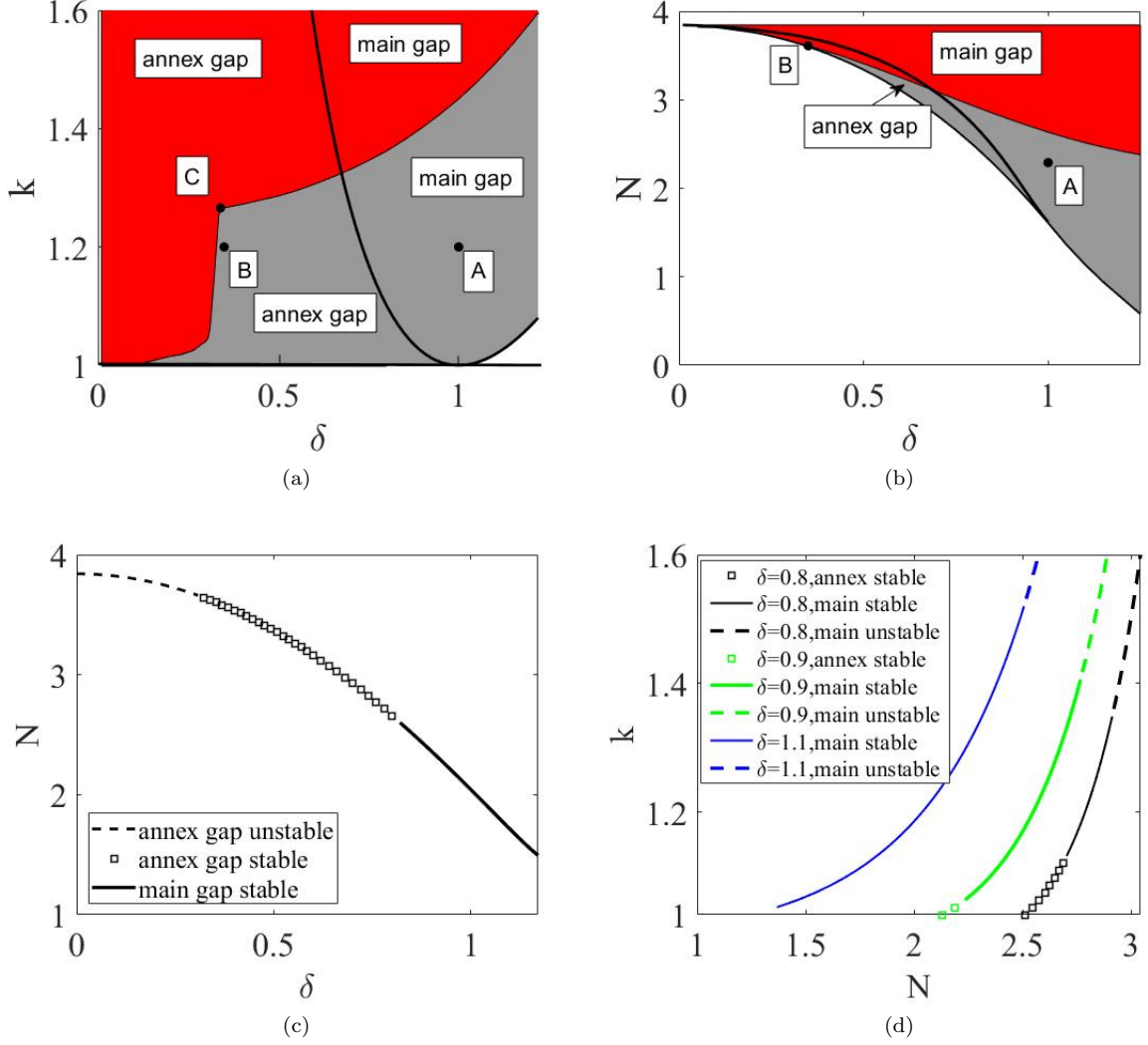


FIG. 9: (a,b): Existence and stability areas for skew-symmetric solitons in the plane of the pseudo-SOC strength (δ) and propagation constant (k) or total norm (N). The parabola-shaped black continuous curve in (a), $k = (\delta^4 + 1) / (2\delta^2)$, see Eqs. (11) and (12), is the boundary between the main and annex spectral gaps at $\delta < 1$, and a border of the main bandgap at $\delta > 1$, where the annex gap does not exist. The boundary between the annex and main gaps is shown in (b) too. Points A and B in (a) and (b) correspond to stable solitons displayed in Figs. 7 and 8, respectively. Symbol C denotes the corner point of the stability boundary, with coordinate $k \approx k_{cr} = 5/4$, see details in the text. The skew-symmetric solitons are unstable, stable, and nonexistent (or not found) in the red, gray, and white areas, respectively. (c) Dependence $N(\delta)$ for the skew-symmetric solitons at a fixed value of the propagation constant, $k = 1.1$. Pursuant to Eq. (13), segment $\delta < 0.801$ belongs to the annex bandgap. (d) Dependence $k(N)$ at fixed values of the pseudo-SOC strength: $\delta = 0.8; 0.9; 1.1$.

In these equations, δ is eliminated by obvious rescaling, once the second derivatives are absent. Accordingly, stationary real equations (6) and (7) are replaced by

$$\frac{dV}{dx} = -kU + U^5 + V, \quad (49)$$

$$\frac{dU}{dx} = kV - V^5 - U. \quad (50)$$

This approximation applies to localized solutions of the underlying system with size $L \sim \delta \gg 1$ (if the coupling constant Λ is not set to be $\Lambda = 1$ by rescaling, see Eqs. (1) and (2), the conditions for the applicability of the approximation are $L \sim \delta/\Lambda$, with $\delta \gg \sqrt{\Lambda}$).

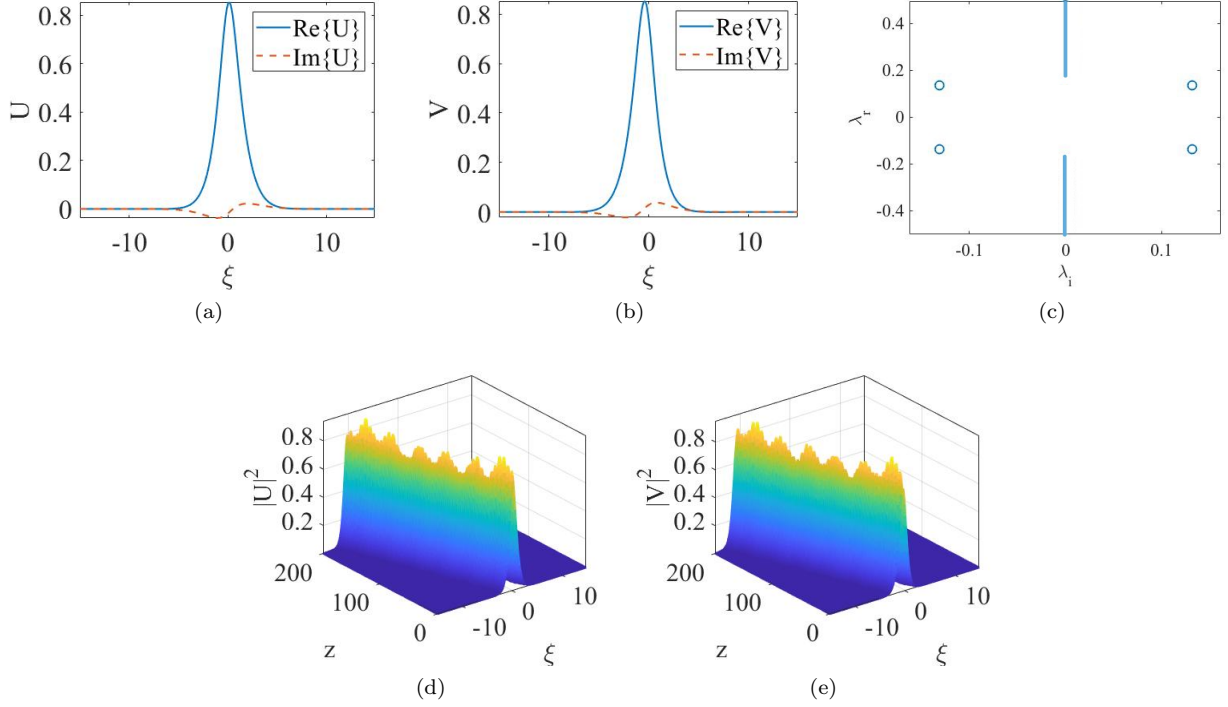


FIG. 10: (a,b): Complex profiles of two components of a soliton with tilt (“velocity”) c , as found in the numerical form from Eqs. (18) and (19). Its propagation constant, pseudo-SOC strength and “velocity” are $k = 1.2$, $\delta = 0.8$ and $c = 0.05$, respectively (c) The spectrum of stability eigenvalues for perturbation modes around the soliton. The vertical stripe with a gap represents the continuous spectrum of real eigenvalues. The quartet of complex eigenvalues accounts for the weak instability which transforms the stationary soliton into a breather. (d,e) The weakly unstable evolution of the soliton shown in (a,b).

The dispersion relation of system (47), (48) is also simplified in comparison with its counterpart (9):

$$k^2 = 1 + q^2. \quad (51)$$

It gives rise to a finite bandgap $k^2 < 1$, in which *gap solitons* may be sought for [63, 64]. In the framework of the full system of Eqs. (3) and (4), this gap may overlap with “remote” branches of the full dispersion relation, but this circumstance will only give rise to decay of the gap solitons at an exponentially small rate.

For tilted solitons, the replacement of x by coordinate (14) transforms Eqs. (47), (48) into

$$\begin{aligned} iu_z - icu_\xi - v_\xi + |u|^4 u + v &= 0, \\ iv_z - icv_\xi + u_\xi + |v|^4 v + u &= 0. \end{aligned} \quad (52)$$

The bandgap generated by Eqs. (52) is $k^2 < 1 - c^2$. Obviously, gap solitons cannot exist for $c^2 > 1$. Detailed consideration of solutions to system (52) is left beyond the scope of the present work.

5.2. Analytical relations

As well as solutions to the system of full equations (6) and (7), Eqs. (49) and (50) are compatible with skew-symmetry and antisymmetry constraints, defined by Eq. (39) and (46). Further, dividing Eq. (49) by Eq. (50) leads to an equation relating fields U and V :

$$\frac{dU}{dV} = -\frac{U - kV + V^5}{V - kU + U^5}. \quad (53)$$

Obvious integration of Eq. (53) yields the following result:

$$h \equiv UV - \frac{k}{2}(U^2 + V^2) + \frac{1}{6}(U^6 + V^6) = 0 \quad (54)$$

(in the general case, Eq. (54) has an arbitrary constant on the right-hand side; the constant is zero for solitons, which have $U(x)$ and $V(x)$ vanishing at $|x| \rightarrow \infty$). In fact, expression (54) is the formal Hamiltonian of Eqs. (49) and (50), the respective canonical representation of these equations being $dV/dx = \partial h/\partial U$, $dU/dx = -\partial h/\partial V$.

It immediately follows from Eq. (54) that solitons subject to the skew-symmetry constraint (39) *cannot exist*, because, at $x = 0$, where Eq. (39) yields $U(x = 0) = V(x = 0)$, Eq. (54) amounts to

$$(1 - k)U^2(x = 0) + \frac{1}{3}U^6(x = 0) = 0, \quad (55)$$

which, obviously, admits solely $U(x = 0) = V(x = 0) = 0$ inside the bandgap, at $k^2 < 1$, and only the trivial solution, $U = V \equiv 0$, may have both components vanishing at $x = 0$. On the other hand, the skew-antisymmetric constraint (46) (which implies $V(x = 0) = -U(x = 0)$) admits the existence of solitons, yielding the following exact value of the fields at $x = 0$:

$$U(x = 0) = -V(x = 0) = [3(1 + k)]^{1/4}. \quad (56)$$

Note that the values given by Eq. (56) do not correspond to maxima of U or $|V|$ (i.e., the maxima are not located at $x = 0$). The maximum of U (but not of $|V|$) corresponds to $dU/dx = 0$, hence Eq. (50) yields, in this case,

$$-kV + V^5 + U = 0. \quad (57)$$

The corresponding values, U_{\max} and V (which does not represent a maximum if $|V|$) should be found from the system of Eqs. (54) and (57). In the general case, it is not possible to solve this system analytically. However, a solution is available in the case of $k = 0$, i.e., at the midpoint of the finite gap:

$$U_{\max}(k = 0) = 5^{5/24} \approx 1.398, \quad V(k = 0) = -5^{1/24} \approx -1.069. \quad (58)$$

Accordingly, at the point of the maximum of $|V(x)|$ the values are $V_{\max}(k = 0) = -5^{5/24} \approx -1.398$, $U(k = 0) = 5^{1/24} \approx 1.069$. For comparison, at the same value of the propagation constant, $k = 0$, Eq. (56) yields a value which is smaller than $U_{\max}(k = 0)$:

$$U(x = 0, k = 0) = -V(x = 0, k = 0) = 3^{1/4} \approx 1.316. \quad (59)$$

Note that Eq. (54) demonstrates that the solution cannot have zeros in one component ($V = 0$ or $U = 0$) at $k < 0$. However, zeros may exist at $k > 0$. Indeed, setting $V = 0$ in Eq. (54), one finds that, at this point, the value of U is

$$U(V = 0) = (3k)^{1/4} \quad (60)$$

(accordingly, $V(U = 0) = -(3k)^{1/4}$), which is relevant at $k > 0$.

Further, the linearized version of Eqs. (49) and (50) yields the following expressions for asymptotic tails of gap solitons:

$$U(x) = U_0 \exp\left(-\sqrt{1 - k^2}|x|\right) \begin{cases} 1, & \text{at } x \rightarrow +\infty, \\ -k^{-1}(1 - \sqrt{1 - k^2}), & \text{at } x \rightarrow -\infty, \end{cases} \quad (61)$$

$$V(x) = U_0 \exp\left(-\sqrt{1 - k^2}|x|\right) \begin{cases} k^{-1}(1 - \sqrt{1 - k^2}), & \text{at } x \rightarrow +\infty, \\ -1, & \text{at } x \rightarrow -\infty, \end{cases} \quad (62)$$

with the exponential-decay rate, $\sqrt{1 - k^2}$, determined by Eq. (51), while constant U_0 is indefinite, in terms of the asymptotic approximation. These expressions comply with the skew-antisymmetry condition (46), and they have a singularity at $k \rightarrow 0$. In the latter limit, Eqs. (62) amount to

$$V_0 \approx (k/2)U_0, \quad \text{at } x > 0, \quad (63)$$

$$U_0 \approx (k/2)V_0, \quad \text{at } x < 0, \quad (64)$$

i.e., at $k = 0$ the asymptotic tail (62) of either field vanishes at positive or negative x . In this case, the correct asymptotic form of the solution, replacing Eqs. (62), is

$$U(x) = \begin{cases} U_0 e^{-x}, & \text{at } x \rightarrow +\infty, \\ (U_0^5/6) e^{5x}, & \text{at } x \rightarrow -\infty, \end{cases} \quad (65)$$

$$V(x) = \begin{cases} -(U_0^5/6) e^{-5x}, & \text{at } x \rightarrow +\infty, \\ -U_0 e^x, & \text{at } x \rightarrow -\infty, \end{cases} \quad (66)$$

where U_0 remains an indefinite constant.

5.3. Soliton solutions

There is a possibility to construct approximate analytical solutions for the skew-antisymmetric gap solitons near the bottom edge of the bandgap, i.e., for

$$0 < 1 + k \equiv \varepsilon \ll 1. \quad (67)$$

In this case, it is convenient to split each component in spatially even and odd parts:

$$\{U(x), V(x)\} = \{U_{\text{even}}(x), V_{\text{even}}(x)\} + \{U_{\text{odd}}(x), V_{\text{odd}}(x)\}. \quad (68)$$

Then, the consideration of Eqs. (49) and (50) suggests that, in the case of small ε , the solitons have large width W and small amplitudes of the even and odd parts, $A_{\text{even,odd}}$, estimated as

$$W \sim \varepsilon^{-1/2}, \quad A_{\text{even}} \sim \varepsilon^{1/4}, \quad A_{\text{odd}} \sim \varepsilon^{3/4}. \quad (69)$$

Taking estimates (69) into account, the consideration of Eqs. (49) and (50) leads, first, to an approximate relation between U_{even} and U_{odd} :

$$U_{\text{odd}} = -\frac{1}{2} \frac{dU_{\text{even}}}{dx}. \quad (70)$$

After elimination of U_{odd} by means of Eq. (70), the remaining equation for $U_{\text{even}}(x)$ is

$$\varepsilon U_{\text{even}} = \frac{d^2 U_{\text{even}}}{dx^2} + 2U_{\text{even}}^5. \quad (71)$$

An obvious soliton solutions to Eq. (71) is

$$U_{\text{even}}^{(\text{sol})}(x) = \frac{(3\varepsilon/2)^{1/4}}{\sqrt{\cosh(2\sqrt{\varepsilon}x)}}, \quad (72)$$

cf. Eq. (24). Then, the odd component of the soliton is produced by the substitution of this in Eq. (70):

$$U_{\text{odd}}^{(\text{sol})}(x) = \frac{1}{2} \left(\frac{3}{2} \varepsilon^3 \right)^{1/4} \frac{\sinh(2\sqrt{\varepsilon}x)}{[\cosh(2\sqrt{\varepsilon}x)]^{3/2}}. \quad (73)$$

Expressions (72) and (73) agree with estimates (69), and the limit value of the total norm of the gap soliton coincides with the TS value (25):

$$N(\varepsilon \rightarrow 0) \equiv 2 \int_{-\infty}^{+\infty} [U_{\text{even}}^2(x) + U_{\text{odd}}^2(x)]_{\varepsilon \rightarrow 0} dx = \sqrt{3/2}\pi \approx 3.85. \quad (74)$$

The numerical solution for gap solitons near the bottom edge of the bandgap produces a profile shown in Fig. 11, which is close to the analytical approximation given by Eqs. (72) and (73). Note that, even in the case of $\varepsilon = 0.01$ displayed in the figure, the soliton's amplitude is not really small.

The numerical solution of the equations produced by the linearization of Eqs. (47) and (48) for small perturbations around the gap solitons yields unstable eigenvalues. This conclusion complies with the above-mentioned conjecture that skew-antisymmetric solitons are subject to instability, all the gap solitons belonging to this type. In the case shown in Fig. 11, the unstable eigenvalues are small and, accordingly, direct simulations demonstrate that the perturbed gap soliton survives long propagation, over the distance exceeding 10 diffraction lengths, hence these solitons are physically relevant states.

Deeper into the bandgap, the shape of the gap solitons becomes sharper, and their instability gets stronger. In particular, at the midpoint of the bandgap, $k = 0$, the numerically found soliton's shape, displayed in Fig. 12, features strong spatial asymmetry mentioned above (see Eqs. (63) and (64)). Its instability develops over the propagation distance exceeding ~ 5 diffraction length. This numerical solution corroborates the exact analytical results given by Eqs. (58) and (59).

The numerical solution produces gap solitons as well at $k > 0$, as shown in Fig. 13. Their shape features zero crossings, in exact agreement with Eq. (60). In this case, the instability is strong, leading to destruction of the soliton after passing $\simeq 1$ diffraction length.

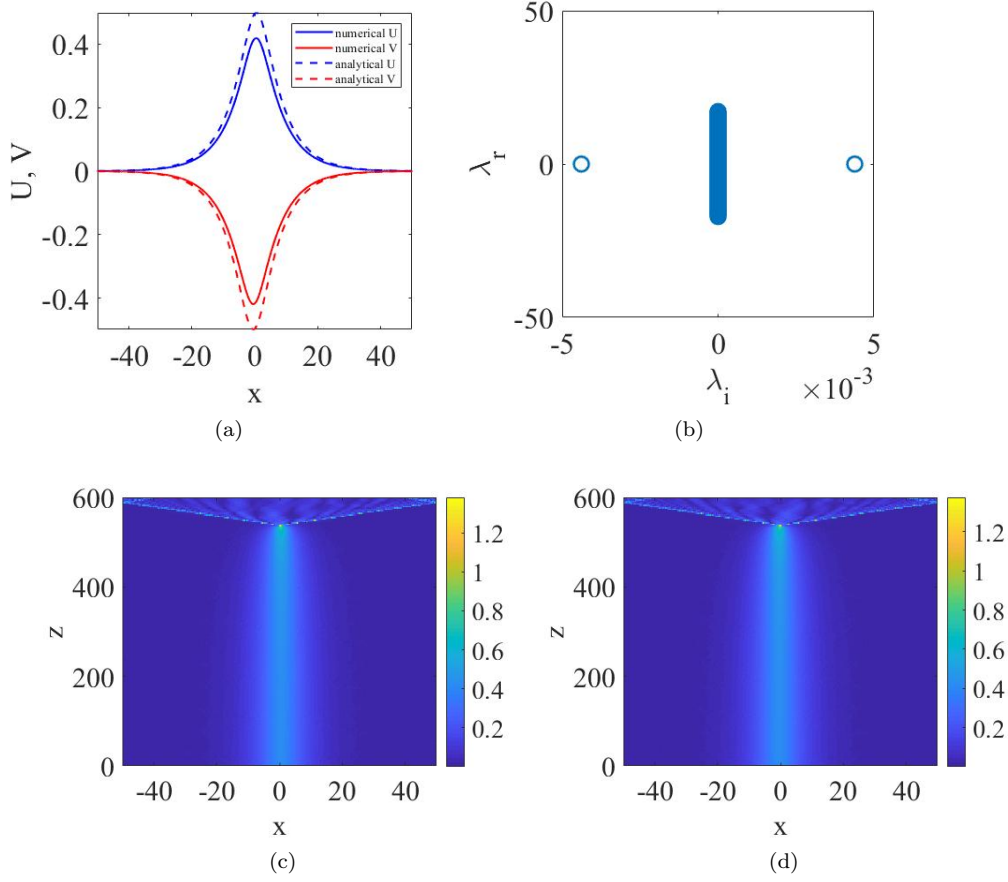


FIG. 11: (a) Numerically found profiles of components U and V of the gap soliton, and their approximate analytical counterparts, given by Eqs. (68), (70), (72) and (46), at $k = -0.99$ (i.e., $\varepsilon = 0.01$ in Eq. (67)). The total norm of the numerical solution is $N \approx 3.78$, to be compared to the TS value (74). (b) The spectrum of stability eigenvalues for small perturbation modes around this soliton. (c,d) Weakly unstable evolution of the soliton shown in (a).

Finally, the gap-soliton family as a whole is characterized by the $k(N)$ dependence, which is shown in Fig. 14, as obtained from the numerical solution. It is worthy to note the difference of this double-value dependence from its monotonous single-value counterpart obtained in the full system, which includes the diffraction terms (second derivatives), cf. Fig. 9(d). The limit value of N corresponding to the bottom of the bandgap, $k = -1$, is given by Eq. (74).

Because the value of the solution with $k = 1$ at $x = 0$, as given by Eq. (56), is finite, $U(x = 0, k = 1) = -V(x = 0, k = 1) = 3 \cdot 2^{1/4}$, and the width of the soliton diverges $\sim (1 - k^2)^{-1/2}$ in the limit of $k \rightarrow 1$, as per Eqs. (62), the integral norm diverges too in this limit.

6. Conclusion

The objective of this work is to expand the recently proposed mechanism for stabilizing TSs (Townes solitons) by means of the linear SOC (spin-orbit-coupling) terms in binary BEC, or ones emulating SOC in other physical settings. In Refs. [42] and [29], this mechanism was elaborated for 2D matter-wave solitons realizing SOC in BEC, and for 2D spatiotemporal optical solitons in dual-core planar waveguides. In both cases, TSs existing in the absence of SOC or quasi-SOC are the usual 2D solitons created in the unstable form by the cubic focusing nonlinearity. Here, we elaborate the mechanism for the stabilization of the 1D variety of TSs, in a two-component system with the quintic self-focusing. This setting may be realized for spatial solitons in a dual-core planar optical waveguides dominated by the quintic nonlinearity, with the SOC-emulating terms represented by skewness in the tunnel coupling between parallel cores of the coupler. The results identify a vast stability region for skew-symmetric two-component solitons, in

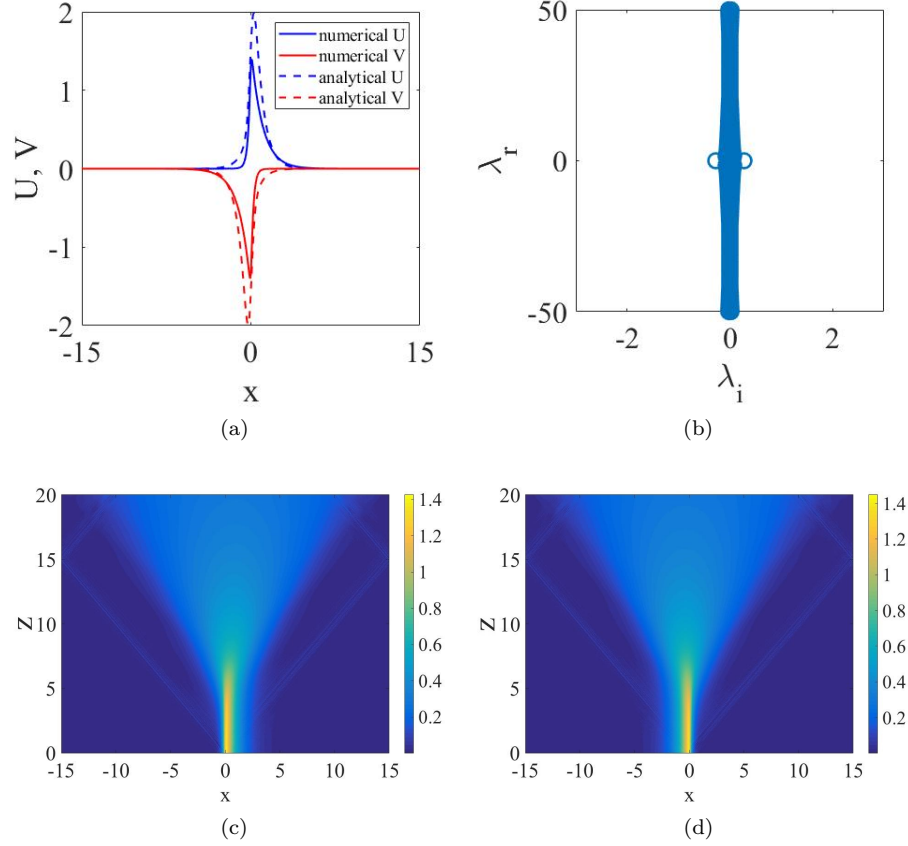


FIG. 12: The same as in Fig. 11, but for the gap soliton with $k = 0$, taken at the midpoint of the bandgap. Values of the fields at $x = 0$ are exactly predicted by Eq. (56). The total norm of this soliton is $N \approx 2.78$, which is essentially smaller than the TS value (74),

the main (semi-infinite) and annex (finite) bandgaps alike. Thus, the SOC-driven stabilization method is a universal one, being applicable to TS in both 2D and 1D settings, with the cubic and quintic nonlinearities, respectively. As a part of the analysis, we have also considered asymmetric solitons in the quintic coupler in the absence of SOC.

An extension of the analysis, also elaborated in this work, is its application to broad solitons, for which the usual diffraction terms are negligible, and the system is simplified to one with a finite bandgap. In this case, some results for the solitons populating the gap can be obtained in an exact analytical form, and a subfamily of the gap solitons near the bottom of the gap is constructed in an approximate analytical form. On the contrary to the full system, the reduced diffractionless one maintains only skew-antisymmetric solitons, which are unstable, although the instability is weak for the solitons constructed near the bandgap's bottom.

The present analysis can be further developed in several directions. In particular, a challenging possibility is to develop a systematic analysis of tilted solitons, in the full and reduced systems alike. Other relevant issues are interactions of solitons in these systems, as well as effects of dissipation.

Acknowledgments

This work was supported, in part, by the Israel Science Foundation through grant No. 1287/17. Z.C. acknowledges an excellence scholarship provided by the Tel Aviv University.

-
- [1] Bergé L. Wave collapse in physics: Principles and applications to light and plasma waves. Phys. Rep. 1998;303:259-372.
 - [2] Fibich G. The Nonlinear Schrödinger Equation: Singular Solutions and Optical Collapse. Springer: Heidelberg, 2015.
 - [3] Chiao RY, Garmire E, Townes CH, Self-trapping of optical beams. Phys. Rev. Lett. 1964;13:479-482.

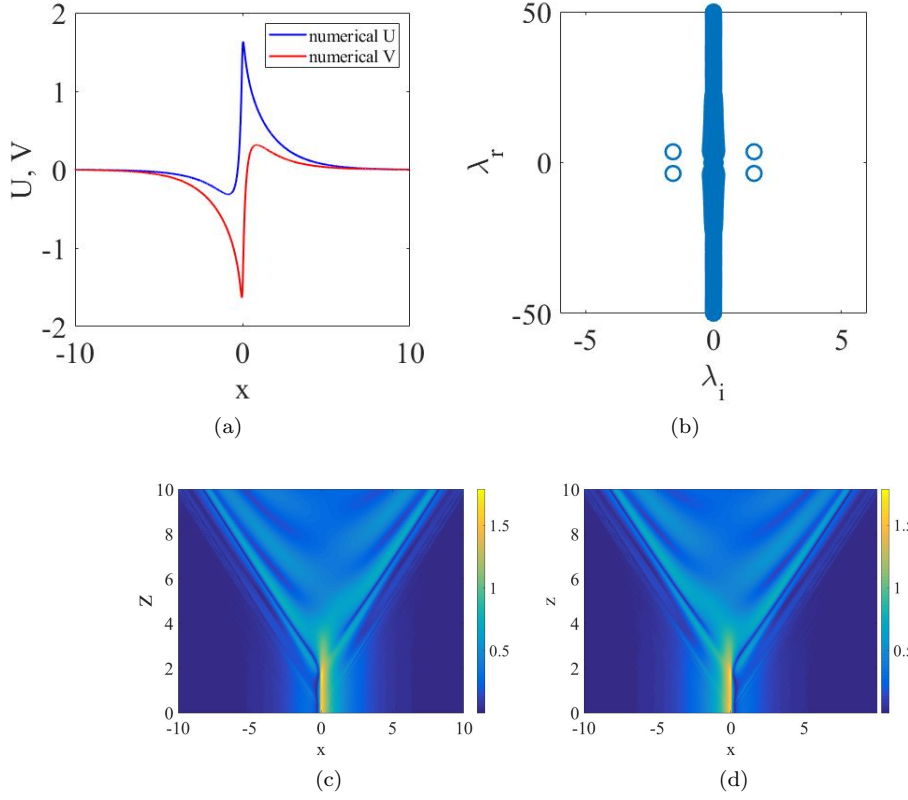


FIG. 13: The same as in Fig. 12, but for the gap soliton close to the top edge of the bandgap, at $k = +0.8$. Values of the fields at the zero-crossing points and at $x = 0$ are exactly predicted, severally, by Eq. (60) and (56). The total norm of the soliton is $N \approx 3.94$, which exceeds the TS value (74).

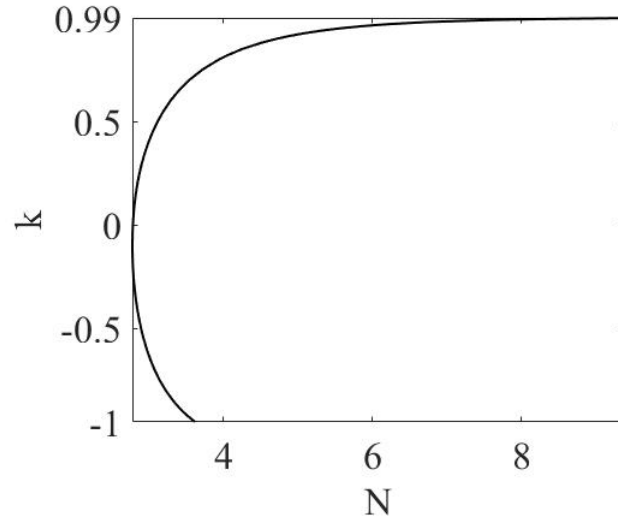


FIG. 14: The numerically found dependence $k(N)$ for the gap-solitons family, produced by the simplified diffractionless system (47), (48).

- [4] Abdullaev FK, Salerno M. Gap-Townes solitons and localized excitations in low-dimensional Bose-Einstein condensates in optical lattices. *Phys. Rev. A* 2005;72:033617.
- [5] Senthilnathan K, Li Q, Nakkeeran K, Wai PKA. Robust pedestal-free pulse compression in cubic-quintic nonlinear media. *Phys. Rev. A* 2008;78:033835.
- [6] Kivshar YS, Agrawal GP. Optical Solitons: From Fibers to Photonic Crystals. San Diego: Academic Press; 2003.
- [7] Robinson PA. Nonlinear wave collapse and strong turbulence. *Rev. Mod. Phys.* 1997;69:507-573.
- [8] Pitaevskii P, Stringari S, Bose-Einstein Condensation, Oxford University Press: Oxford, 2003.
- [9] Malomed BA, Mihalache D, Wise F, Torner L. Spatiotemporal optical solitons. *J. Optics B* 2005;7:R53–R72.
- [10] Mihalache D. Three-dimensional dissipative optical solitons. *Cent. Eur. J. Phys.* 2008;6:582-587.
- [11] Malomed BA, Mihalache D, Wise F, Torner L. Viewpoint: On multidimensional solitons and their legacy in contemporary atomic, molecular and optical physics. *J. Phys. B: At. Mol. Opt. Phys.* 2016;49:170502.
- [12] Malomed BA. Multidimensional solitons: Well established results and novel findings. *Eur. Phys. J. Special Top.* 2016;225:2507-2532.
- [13] Kartashov Y, Astrakharchik G, Malomed B, Torner L. Frontiers in multidimensional self-trapping of nonlinear fields and matter. *Nature Reviews Physics* 2019;1:185-197; <https://doi.org/10.1038/s42254-019-0025-7>.
- [14] Quiroga-Teixeiro M, Michinel H. Stable azimuthal stationary state in quintic nonlinear optical media. *J. Opt. Soc. Amer. B* 1997;14:2004-2009.
- [15] Falcão-Filho, de Araújo CB, Boudebs G, Leblond H, Skarka V. Robust two-dimensional spatial solitons in liquid carbon disulfide. *Phys. Rev. Lett.* 2013;110:013901.
- [16] Reyna AS, de Araújo CB. High-order optical nonlinearities in plasmonic nanocomposites – a review. *Adv. Opt. Phot.* 2017;9:720-774.
- [17] Baizakov BB, Malomed BA, Salerno M. Multidimensional solitons in periodic potentials. *Europhys. Lett.* 2003;63:642-648.
- [18] Yang J, Musslimani ZH. Fundamental and vortex solitons in a two-dimensional optical lattice. *Opt. Lett.* 2003;28:2094-2096.
- [19] Petrov DS. Quantum mechanical stabilization of a collapsing Bose-Bose mixture. *Phys. Rev. Lett.* 2015;115:155302.
- [20] Petrov DS, Astrakharchik GE. Ultradilute low-dimensional liquids. *Phys. Rev. Lett.* 2016;117:100401.
- [21] Žin P, Pylak M, Wasak T, Gajda M, Idziaszek Z. Quantum Bose-Bose droplets at a dimensional crossover, *Phys. Rev. A* 2018;98:051603(R).
- [22] Ilg T, Kumlin J, Santos L, Petrov DS, Buchler HP. Dimensional crossover for the beyond-mean-field correction in Bose gases. *Phys. Rev. A* 2018;98: 051604.
- [23] Lee TD, Huang K, Yang CN. Eigenvalues and eigenfunctions of a Bose system of hard spheres and its low temperature properties. *Phys. Rev.* 1957; 106: 1135-1145.
- [24] Cabrera C, Tanzi L, Sanz J, Naylor B, Thomas P, Cheiney P, Tarruell L, Quantum liquid droplets in a mixture of Bose-Einstein condensates. *Science* 2018;359:301-304.
- [25] Cheiney P, Cabrera CR, Sanz J, Naylor B, Tanzi L, Tarruell L. Bright soliton to quantum droplet transition in a mixture of Bose-Einstein condensates. *Phys. Rev. Lett.* 2018;120:135301.
- [26] G. Semeghini, G. Ferioli, L. Masi, C. Mazzinghi, L. Wolswijk, F. Minardi, M. Modugno, G. Modugno, M. Inguscio, M. Fattori. Self-bound quantum droplets of atomic mixtures in free space. *Phys. Rev. Lett.* 2018;120:235301.
- [27] Ferioli G, Semeghini G, Masi L, Giusti G, Modugno G, Inguscio M, Gallemi A, Recati A, Fattori M. Collisions of self-bound quantum droplets. *Phys. Rev. Lett.* 2019;122:090401.
- [28] C. D’Errico, A. Burchianti, M. Prevedelli, L. Salasnich, F. Ancilotto, M. Modugno, F. Minardi, C. Fort. Observation of quantum droplets in a heteronuclear bosonic mixture. *Phys. Rev. Research* 2019;1:033155.
- [29] Kartashov YV, Malomed BA, Tarruell L, Torner L. Three-dimensional droplets of swirling superfluids. *Phys. Rev. A* 2018;98:013612.
- [30] Li Y, Chen Z, Luo Z, Huang C, Tan H, Pang W, Malomed BA. Two-dimensional vortex quantum droplets. *Phys. Rev. A* 2018;98:063602.
- [31] H. Kadau, M. Schmitt, M. Wentzel, C. Wink, T. Maier, I. Ferrier-Barbut, and T. Pfau, Observing the Rosenzweig instability of a quantum ferrofluid. *Nature* 2016;530:194-197.
- [32] M. Schmitt, M. Wenzel, 491 F. Bottcher, I. Ferrier-Barbut and T. Pfau. Self-bound droplets of a dilute magnetic quantum liquid. *Nature* 2016;539:259-262.
- [33] Wachtler F, Santos L. Ground-state properties and elementary excitations of quantum droplets in dipolar Bose-Einstein condensates. *Phys. Rev. A* 2016;94:043618.
- [34] Baillie D, Blakie PB. Droplet crystal ground states of a dipolar Bose gas. *Phys. Rev. Lett.* 2018;121:195301.
- [35] Cidrim A, dos Santos FEA, Henn EAL, Macrì T. Vortices in self-bound dipolar droplets. *Phys. Rev. A* 2018;98:023618.
- [36] Lin YJ, Jimenez-Garcia K, Spielman IB. Spin-orbit-coupled Bose-Einstein condensates. *Nature* 2011;471:83-86.
- [37] Goldman N, Juzeliūnas G, Öhberg P, Spielman IB. Light-induced gauge fields for ultracold atoms. *Rep. Progr. Phys.* 2014;77:126401.
- [38] Zhai H. Degenerate quantum gases with spin-orbit coupling: a review. *Rep. Progr. Phys.* 2015;78:026001.
- [39] Adams EN, Blount EI. Energy bands in the presence of an external force field-II. Anomalous velocities. *J. Phys. Chem. Solids* 1959;10:286-303.
- [40] Mardonov Sh, Sherman EYa, Muga JG, Wang H-W, Ban Y, Chen X. Collapse of spin-orbit-coupled Bose-Einstein condensates. *Phys. Rev. A* 2015;91:043604.
- [41] Li J, Malomed BA, Li W., Chen X., Sherman EYa. Coupled density-spin Bose-Einstein condensates dynamics and collapse in systems with quintic nonlinearity. *Communications in Nonlinear Science and Numerical Simulation.* 2020;82:105045.

- [42] Sakaguchi H, Li B, Malomed BA. Creation of two-dimensional composite solitons in spin-orbit-coupled self-attractive Bose-Einstein condensates in free space. *Phys. Rev. E* 2014;89:032920.
- [43] Sakaguchi H, Sherman EYa, Malomed BA. Vortex solitons in two-dimensional spin-orbit coupled Bose-Einstein condensates: Effects of the Rashba-Dresselhaus coupling and the Zeeman splitting. *Phys. Rev. E* 2016;94:032202.
- [44] Kartashov YV, Torner L, Modugno M, Sherman EYa, Malomed BA, and Konotop VV. Multidimensional hybrid Bose-Einstein condensates stabilized by lower-dimensional spin-orbit coupling. *Phys. Rev. Research* 2020;2:013036.
- [45] Zhang YC, Zhou ZW, Malomed BA, Pu H. Stable solitons in three dimensional free space without the ground state: Self-trapped Bose-Einstein condensates with spin-orbit coupling. *Phys. Rev. Lett.* 2015;115:253902.
- [46] Kartashov YV, Malomed BA, Konotop VV, Lobanov VE, Torner L. Stabilization of solitons in bulk Kerr media by dispersive coupling. *Opt. Lett.* 2015;40:1045-1048.
- [47] Sakaguchi H, Malomed BA. One- and two-dimensional solitons in \mathcal{PT} -symmetric systems emulating spin-orbit coupling. *New J. Phys.* 2016;18:105005.
- [48] Albuch L, Malomed B A. Transitions between symmetric and asymmetric solitons in dual-core systems with cubic-quintic nonlinearity. *Mathematics and Computers in Simulation* 2007;74:312-322.
- [49] Wright EM, Stegeman GI, Wabnitz S. Solitary-wave decay and symmetry-breaking instabilities in two-mode fibers. *Phys. Rev. A* 1989;40:4455.
- [50] Paré C, Florjańczyk M. Approximate model of soliton dynamics in all-optical fibers. *Phys. Rev. A* 1990;41:6287-6295.
- [51] Maimistov AI. Propagation of a light pulse in nonlinear tunnel-coupled optical waveguides. *Sov. J Quantum Electron* 1991;21:687-690.
- [52] Romagnoli M, Trillo S, Wabnitz S. Soliton switching in nonlinear couplers. *Opt Quantum Electron* 1992;24:1237-1267.
- [53] Chu PL, Malomed BA, Peng GD, Skinner I. Soliton dynamics in periodically modulated directional couplers. *Phys. Rev. E* 1994;49:5763-5767.
- [54] Malomed BA. Solitons and nonlinear dynamics in dual-core optical fibers. In: *Handbook of Optical Fibers* (Peng GD, editor), Springer; 2018.
- [55] Landau LD, Lifshitz EM. *Quantum Mechanics*. Nauka Publishers: Moscow, 1974.
- [56] Mayteevaryunoo T, Malomed BA, Dong G. Spontaneous symmetry breaking in a nonlinear double-well structure. *Phys. Rev. A* 2008;78:053601.
- [57] Vakhitov NG, Kolokolov AA. Stationary solutions of the wave equation in a medium with nonlinearity saturation. *Radio-phys. Quantum Electron.* 1973;16:783-789.
- [58] Yang J. *Nonlinear Waves in Integrable and Nonintegrable Systems* SIAM: Philadelphia, 2010.
- [59] Mayteevaryunoo T, Malomed BA. Skew-symmetric vortices and solitons in crossed-lattice potentials. *J. Opt. A: Pure Appl. Opt.* 2009;11:094015.
- [60] Fan Z, Shi Y, Liu Y, Pang W, Li Y, Malomed BA. Cross-symmetric dipolar-matter-wave solitons in double-well chains. *Phys. Rev. E* 2017;95:032226.
- [61] Li Y, Liu Y, Fan Z, Pang W, Fu S, Malomed BA. Two-dimensional dipolar gap solitons in free space with spin-orbit coupling. *Phys. Rev. A* 2017;95:063613.
- [62] Sakaguchi H, Malomed BA. One- and two-dimensional gap solitons in spin-orbit-coupled systems with Zeeman splitting. *Phys. Rev. A* 2018;97:013607.
- [63] Chen W, Mills DL. Gap solitons and the nonlinear optical response of superlattices. *Phys. Rev. Lett.* 1987;58:160-163.
- [64] de Sterke CM, Sipe JE. Gap solitons. *Progr. Optics* 1994;33:203-260.